Applied Surface Science 676 (2024) 161002

Contents lists available at ScienceDirect

Applied Surface Science

journal homepage: www.elsevier.com/locate/apsusc

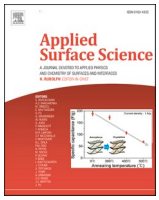

Full Length Article

Plasma-enabled growth of vertically oriented carbon nanostructures for AC line filtering capacitors

N. Bundaleska [a,*], E. Felizardo [a], N.M. Santhosh [b,c], K.K. Upadhyay [d,e], N. Bundaleski [f], O.M.N.D. Teodoro [f], A.M. Botelho do Rego [g,h], A.M. Ferraria [g,h], J. Zavašnik [b,c], U. Cvelbar [b,c], M. Abrashev [i], J. Kissovski [i], A. Mão de Ferro [d], B. Gonçalves [a], L.L. Alves [a], M.F. Montemor [e], E. Tatarova [a,*]

[a] Instituto de Plasmas e Fusão Nuclear (IPFN), Instituto Superior Técnico, Universidade de Lisboa, Lisboa 1049, Portugal
[b] Department of Gaseous Electronics F6, Jožef Stefan Institute, Ljubljana 1000, Slovenia
[c] Jožef Stefan International Postgraduate School, Ljubljana 1000, Slovenia
[d] Charge2C-NewCap, Av. José Francisco Guerreiro, n°28 Paiã Park, Armazém A2.12, 1675-078 Pontinha – Odivelas, Portugal
[e] Centro de Química Estrutural-CQE, Departamento de Engenharia Química, Instituto Superior Técnico, Universidade de Lisboa, 1049-001 Lisboa, Portugal
[f] CEFITEC, Departamento de Física, Faculdade de Ciências e Tecnologia, Universidade Nova de Lisboa, 2829-516 Portugal
[g] BSIRG, iBB, DEQ, Instituto Superior Técnico, Universidade de Lisboa, Lisboa 1049-001, Portugal
[h] Associate Laboratory i4HB—Institute for Health and Bioeconomy at Instituto Superior Técnico, Universidade de Lisboa, 1049-001 Lisboa, Portugal
[i] Faculty of Physics, Sofia University, 1164 Sofia, Bulgaria

ARTICLE INFO

Keywords:
Vertically oriented carbon nanostructures
Microwave plasma growth
Binder-free electrodes
Plasma post-synthesis N-doping
High-frequency AC filtering capacitors

ABSTRACT

Self-standing vertically oriented carbon nanostructures (VCNs) were synthesized using a large-scale microwave plasma under low-pressure conditions, employing methane as a carbon precursor. The influence of plasma operational and substrate conditions on nanostructure growth and morphology were systematically studied. Furthermore, post-synthesis N-doping of VCNs with nitrogen content of 2.4 *at% N* was achieved using an Ar-N_2 microwave plasma. Plasma-enabled direct deposition of VCNs, both doped and un-doped, onto nickel foils has been accomplished. The assessment of the developed nanostructures as electrodes in high-frequency AC filtering capacitors, has demonstrated an overall capacitance of approximately 480 μF at 100 Hz, with a cut-off frequency of 4 kHz for a phase angle of −45°. The excellent electrochemical performance can be attributed to the appropriate structural and morphological properties peculiar for the directly deposited on nickel foil VCNs providing binder-free electrode fabrication, thus enhancing the electrode's conductivity and charge transfer kinetics. This plasma-enabled approach for electrode design on a large scale, coupled with excellent filtering performance, paves the way for many applications in high-frequency scenarios, offering an environmentally friendly alternative to conventional electrolytic capacitors.

1. Introduction

Much research interest has been shown in vertically oriented carbon nanostructures (VCNs), such as graphene and its derivatives – vertical graphene (VG) sheets, nanotubes (CNT), nanofibers (CNF), nanorods, etc. Due to their exceptional morphological and structural features, these materials are of interest for a wide range of potential applications. Plasma-enhanced chemical vapor deposition (PECVD) techniques have been widely implemented to fabricate such vertical structures aligned perpendicularly on a substrate with open edges representing a 3D ordered network of carbon nanostructures [1–7]. In general, VCNs possess some advantages over their horizontal or randomly spaced variants, such as improved mechanical stability, improved accessibility, exposure to long, thin, reactive edges, etc. For example, VG sheets possess better mechanical stability compared to free-standing graphene due to their attachment to a substrate, thus forming a network with different morphologies. The vertical architecture also prevents agglomeration, which is a serious problem in randomly placed graphene sheets, where the strong π-π stacking and van der Waals interactions lead to restacking [1,8–10]. Similar to graphene, the free-standing CNTs with

* Corresponding authors.
E-mail addresses: neli.bundaleska@tecnico.ulisboa.pt (N. Bundaleska), elena.stefanova@tecnico.ulisboa.pt (E. Tatarova).

https://doi.org/10.1016/j.apsusc.2024.161002
Received 16 May 2024; Received in revised form 26 July 2024; Accepted 15 August 2024
Available online 16 August 2024

heavily entangled bundles, results in intrinsic difficulties concerning dispersion and permeation, and limits their application in several systems such as membrane fillers for gas purification [11]. In contrast, in the vertical configuration, the large surface area of graphene is preserved with open boundaries, allowing easy access to the graphene sheets by ions, gas, or liquid molecules. For example, the high aspect ratio and easily accessible reactive sites are of crucial importance for electrochemical devices and sensors. Therefore, to take the advantage of morphological and excellent electrical properties, VG configurations can be grown directly on a conductive substrate and used as an advanced material for various applications, such as electrochemical and energy storage devices, sensors, supercapacitors in alternating current (AC) filtering, field emission, purification, electrocatalysts towards hydrogen evolution reaction (HER) etc. [2,6,9,12–17]. The direct growth of VCN on conductive substrate is advantageous because it provides binder-free electrode fabrication, thus enhancing the electrode's conductivity and charge transfer kinetics [12]. Generally, a PECVD synthesis of VCN involves plasma driven dissociation and ionization of carbon precursors, followed by self-aligned deposition of the carbon species on a substrate at specific conditions. The benefits of plasma in advanced nanomaterial synthesis are well recognized, as one of the potential green techniques for controlled synthesis and assembly of nanostructures [1–6]. Plasmas provide a highly reactive medium that contains electrons, energetic ions, free radicals, excited atoms and molecules, photons etc. All these particles partake in the synthesis process by contributing to the substrate surface activation, precursor dissociation and ionization, elevation of the substrate temperature, reducing the thresholds for surface reactions etc. There are several plasma sources reported (microwave (MW), radiofrequency (RF), direct current (dc) and other combinations) operating at different pressures for VCN fabrication [16]. Additionally, plasma-enabled techniques offer the structure-controlled synthesis of VCN and VG structures with desired morphology and orientations [19]. This phenomenon is attributed to the electric fields inherently associated with the plasma sheath created at the substrate interface. Also, PECVD allows the growth process on different substrates at lower substrate temperatures as compared to classical CVD, which widens the choice of substrate materials [20]. Growth of CNFs on borosilicate glass by DC PECVD system at temperatures as low as 90 °C has been reported [7]. For the synthesis of VGs, temperatures around 400 °C have been reported as the lowest, and demonstrating that the structure quality and the growth rate are increasing with temperature [1,21].

The growth mechanism of VGNs in PECVD has been analyzed experimentally and theoretically by many research groups [22–24], indicating that the process proceeds with the creation of radicals in the plasma, their interaction with the substrate surface, nucleation, coalescence of C radicals and vertical growth. Numerous factors are known to have an impact on the growth process. They can be divided into two groups: one associated with substrate conditions (temperature, substrate material, presence of a catalyst), and other related to the plasma operational conditions (power, carbon precursor flow rate, mixture composition, substrate location in plasma environment, deposition time, bias voltage etc.) [1,7–11]. It is commonly accepted that the first step is the substrate surface activation by plasma provided ion bombardment, leading to the formation of defects and dangling bonds, which attract radicals from the plasma. Consequently, a thin buffer layer, consisting of both amorphous and graphitic carbon, parallel to the substrate is deposited, which serves as a base for the carbon nucleation. Later, vertical growth continues by surface diffusion of deposited carbon atoms. Gaseous carbon-containing precursors such as CH_4, C_2H_2, CO, and C_3H_4 mixed with H_2 or O_2 are commonly used, although experiments with liquid and solid precursors (butter, honey, C_{60} etc.) can also be found in the literature [1,7,9,18]. In addition to the synthesis process, plasmas also provide a possibility for the controlled surface engineering of carbon by easy functionalization, and heteroatom doping, which can be achieved either by in situ (simultaneous growth and doping) or post-treatment (doping of previously synthesized VCNs) methods [25–28]. These surface engineering methods by molecular and atomic doping can be used as a potential technique to tailor the electrical and electrochemical properties of VCNs [29,30].

Among the various possible applications of VCNs, there is strong interest in the development of supercapacitor (SC) electrodes operating at high frequencies for AC filtering in order to replace bulky aluminum electrolytic capacitors [31–33]. Circuit elements with high-frequency capacitive response are of technological importance in a wide range of applications in the fields of conventional and power electronics, e.g. for passing or bypassing low frequency signals (mostly used for ripple and noise filtering), decoupling in power supplies, DC link circuits, power factor corrections etc. In AC filtering applications, the US/EU 60/50 Hz line frequency are used, thus, the filtering capacitor, following the full-wave rectifier, must capacitively respond at 120/100 Hz and with a minimum loss (thermal generation) [31]. At such frequency, conventional electrochemical capacitors (ECs) generally lose their capacitive characteristics, instead, they behave like highly lossy inductors with a positive impedance phase angle. For that reason, most of the market share for this application is dominated by electrolytic capacitors, which work well in this range of frequencies. However, the low capacitance values, in the order of μF, and bulky sizes of these types are limiting their application in the downscaling of circuit boards, in particular for portable electronics. Therefore, a highly desired aspect in today's growing technological market is to bridge the performance gap between the capacitance and frequency response between electrochemical and electrolytic capacitors, which will bring great impacts on compact circuit design, with the use of miniaturized electrolytic capacitors, self-powered tiny sensor systems etc.

To this end, plasma synthesis of vertically oriented carbon nanostructures (VCN) provides a scalable and flexible approach offering control over nanostructure morphology and composition. Nevertheless, each plasma has its own particular properties and even two plasma reactors based on the same design usually have different outcomes for the same operating parameters. Applied to this particular case, the consequence is that similar plasma sources can favour VCN with rather different morphology, interlayer distance, thickness, uniformity etc., depending on the plasma parameters [1,2]. The general aim of the present investigation is to explore the overall capabilities of a large-scale slot antenna excited microwave plasma reactor developed at IPFN for the growth of carbon nanostructures under low-pressure conditions using methane as a carbon precursor in terms of its chemical, morphological and electrical properties. Moreover, the specific goal is to determine the optimal conditions for the growth of VCN for direct use as electrodes in AC filter capacitors. To this end the effects of precursor flow rate, substrate material, substrate voltage, gas composition, and substrate pre-treatment were systematically investigated. Additionally, to test the effect of the nitrogen doping on the electrodes additional post deposition treatments of synthesized layers with nitrogen plasma have been conducted. Post-synthesis nitrogen doping of VCNs was achieved within the same plasma reactor system, with a nitrogen content of 2.4 *at % N* determined by X-ray photoelectron spectroscopy (XPS). The VCN and nitrogen-doped VCN with optimal thickness and surface structures deposited on nickel foils were tested as electrodes of AC filtering capacitors, demonstrating excellent capacitive response at high frequencies.

2. Experimental arrangements

2.1. Plasma synthesis of VCNs

A slot antenna excited plasma source based on surface wave propagation is used to fabricate VCN (Fig. 1) [27,34]. The discharge vessel is a glass tube (diameter $D = 24$ cm and length $L = 70$ cm), with a 10 mm-thick quartz window at the top. The plasma chamber was evacuated to provide a base pressure of about 10^{-6} mbar. Argon with high purity (99.999 %) was used as a background gas. Methane injected at the

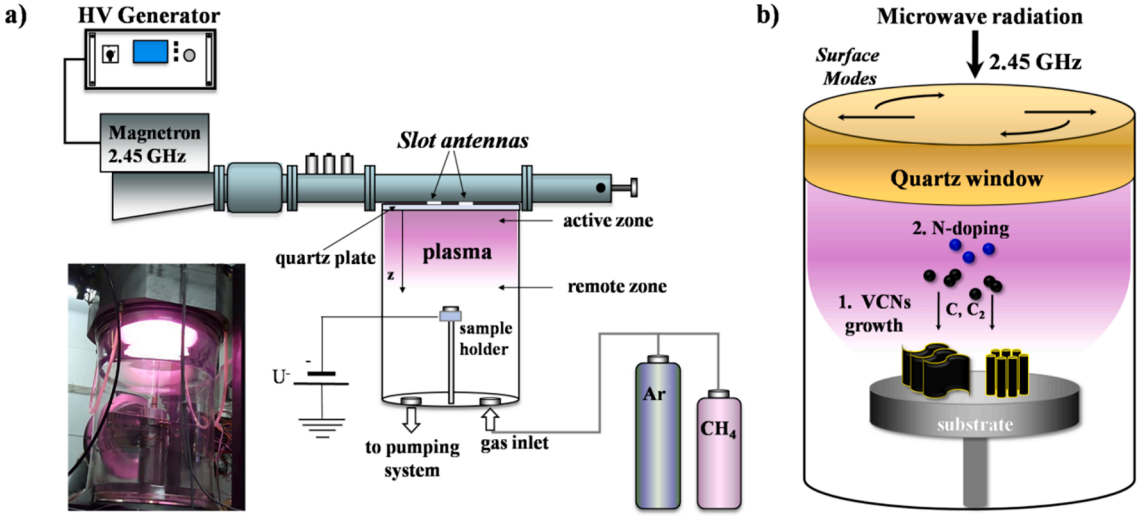

Fig. 1. a) scheme and photo of the experimental setup for the synthesis of vcn; b) scheme of n-doping process using the same plasma reactor.

bottom of the chamber was used as a carbon precursor. The microwave power of 800 W at 2.45 GHz is delivered to the chamber by a waveguide system with a rectangular cross section. The chamber is isolated from the generator by a high-power circulator with a high-power matched load connected to its third port. An impedance transformer matches the chamber impedance to the feeding waveguide. The waves enter the chamber through two slot antennas, which are cut on the wider side of the waveguide. The waveguide is short-circuited from one end, and by tuning, a standing wave pattern is created inside the waveguide with a maximum of the electric field at the antennás position. The plasma is created by the energy carried by surface waves propagating radially and azimuthally along the interface between the plasma and a quartz dielectric plate. The power of the surface wave close to the interface sustains overdense plasma. The microwave electric field decreases exponentially with the distance from the interface and vanishes at some axial distance. Two different regions can be identified concerning the main mechanisms governing plasma production and sustainment. The first one is the discharge zone close to the interface (at about 1 cm from the quartz plate for the present conditions), where the surface waves are propagating, and their energy sustains the discharge. Due to diffusion, the plasma expands into a second "microwave electric field free" remote plasma region. As a rule, the axial length of the remote zone is much larger than that of the active discharge zone. Particle diffusion and heavy particle collisional processes are dominating in this region.

Two types of Ni substrates were used, i.e., Ni-foam and Ni-foil. Before plasma growth, the substrates were subjected to different pre-treatment procedures: the Ni-foam was cleaned with ethanol, followed by annealing at 400 °C for 30 min in air or Ar atmosphere. The Ni-foil substrates were chemically etched in 2 M HCl solution for 1 min, cleaned with deionised water, and dried. In addition, stainless steel was also used as a substrate material. The substrate, placed on a sample holder, was fixed in the remote plasma zone at z = 5 cm from the quartz plate (z-axis is shown in Fig. 1a). The substrate holder includes a brass disc and copper wire, both isolated to secure electrical contact and provide appropriate electrical field distribution. The negative bias voltage (U) was regulated by a high-voltage supply.

The influence of operating conditions such as processing time (t = 1–60 min), carbon precursor flow rate (Q_{CH4} = 5–10 sccm) and microwave power (P = 600–800 W) on the process of VCN growth, was investigated. The bias on the substrate was varied from 0 to −400 V. CH_4 was used as a carbon precursor and its mixtures with H_2 were also used. Prior to all experiments, the reactor was cleaned with Ar plasma at P = 600 W for 60 min. Furthermore, post-synthesis N-doping of the VCN was achieved using the same plasma reactor (Fig. 1b). For this reason, the deposited VCNs were processed at different treatment times in Ar/N_2 plasma environment where large number of nitrogen atoms is created as a result of the N_2 dissociation. The N atoms attach mainly at the reactive edges of the vertically grown nanostructures.

2.2. Characterization techniques

Scanning Electron Microscopy (SEM) characterization of the grown structures was performed by a JEOL, JSM-7001F field emission gun scanning electron microscope operating in secondary electron imaging mode (SEI) using 15 kV accelerating voltage and dual-beam SEM-focused ion beam microscope (FIB-SEM, Helios NanoLab 650i, FEI). The samples were attached to a double-sided adhesive carbon tape mounted on an aluminium stub.

Raman spectroscopy characterization using a LabRAM HR Visible (Horiba Jobin-Yvon) Raman spectrometer at 633 nm with 1 cm^{-1} spectral resolution and a laser spot size of 2 μm was conducted. Measurements were performed with a laser power P=0.054 mW to avoid overheating. Raman spectra from different arbitrarily chosen regions on the sample were collected.

X-ray Photoelectron Spectroscopy (XPS) surface characterization of the Ni-foam substrate and nitrogen-doped VCNs was performed with a XSAM800 non-monochromatic dual anode spectrometer from KRATOS. The spectrum was obtained with Al Kα radiation, at a take-off angle of 45°. Charge shift correction was performed using as a reference the binding energy (BE) of Ni^0, centred at 852.6 eV [35] for the Ni-foam substrate and the BE of sp^2 carbon atoms, C–C or C–H, found in graphene, centred at 284.4 eV [36], for the N-doped VCN. The sensitivity factors used for the quantification were 0.278 (C 1 s), 0.477 (N 1 s), 4.044 (Ni 2p), 0.780 (O 1 s), and 0.328 (Si 2p).

XPS characterization of VCNs on Ni-foam and foil were performed on a VSW XPS system with the Class 100 energy analyzer being a part of a customized experimental setup, assembled for surface investigation by different techniques. Survey spectra were taken in a fixed analyzer transmission mode with a pass energy of 44 eV (FAT 44), energy step of 0.5 eV, and dwell time of 0.5 s. Detailed spectra were taken in FAT22 mode with energy step 0.1 eV and dwell time 4 s per scan. Analysis was performed using the non-monochromatic Mg Kα source (photon energy of 1253.6 eV). The energy was calibrated to the peak position of Ag $3d_{5/2}$ (binding energy of 368.22 eV) and Au $4f_{7/2}$ (binding energy of 83.96 eV) lines.

2.3. Electrochemical measurements

The electrochemical features of the plasma-designed VCN have been investigated in order to reveal their potential as electrodes for supercapacitors. The VCN synthesised directly on the Ni-foil at the plasma conditions P = 800 W, Q_{CH4} = 10 sccm, t = 60 min, U=-400 V, and their 2.4 % N-doped derivatives (NVCN) were used in these experiments. The measurements were performed in a symmetric cell setup using a 6 M KOH electrolyte with 14 mm disk-shaped electrodes, in which the Ni substrate was used as the current collector. The initial assessment of the electrode structures was evaluated by analysing the voltage dependence on the current density, measured in Ag^{-1} (CV studies). Additional analyses using Electrochemical Impedance Spectroscopy (EIS) were performed, to study, particularly, the behaviour of the system at 100 Hz, which is of interest for AC filtering applications.

3. Results and discussion

The growth of VCNs is the result of the interplay between the substrate characteristics and the plasma parameters. Initial surface conditions such as thermal and electronic conductivity, adhesion, surface roughness, and ability to adsorb hydrocarbon species, are found to affect

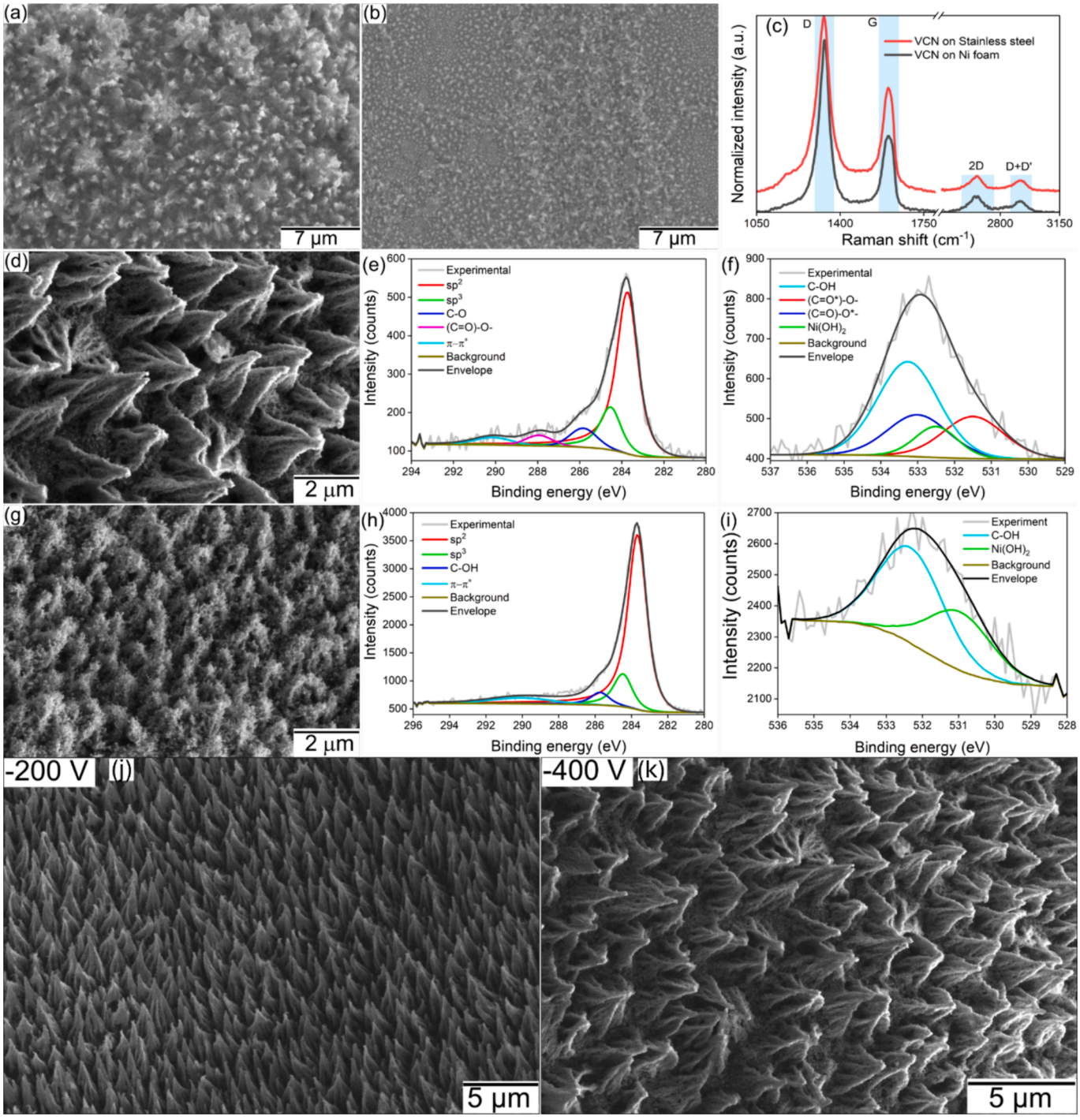

Fig. 2. SEM of VCN synthesized on a) Ni-foam; b) on stainless steel; c) Raman spectra of the two deposits after removing the background; d,e,f) SEM and XPS of VCNs synthesized on air annealed Ni-foam; g,h,i) SEM and XPS of VCNs synthesized on chemically etched Ni-foil; j,k) Effect of substrate bias on the morphology of VCNs.

the growth process [37–40]. In parallel, plasma operational parameters (e.g. power, gas composition and pressure, exposure time) strongly influence the plasma-surface interactions, and consequently the morphology and composition of the assembled structures [1–5]. Besides, as demonstrated plasma also has the potential to dope the previously grown structures tuning their electrical and optical properties.

3.1. Influence of the substrate on the growth process

In the first stage of this study, the influence of the substrate such as substrate type, pre-treatment, and dc biasing of the substrate, on the growth and morphology of synthesized VCN was investigated.

3.1.1. The effect of substrate type

VCNs were deposited on Ni-foam and stainless steel substrates. The deposition of VCNs for both substrates was performed under the same operational conditions (P = 800 W, Q_{CH4} = 10 sccm, p = 0.3 mbar, U = -400 V, t = 60 min). A much thicker deposition was observed on Ni substrate as compared to the stainless steel. Indeed, SEM analysis of the nickel foam reveals the formation of well-defined VCNs with high aerial density and heights of a few microns (Fig. 2a). The structures grown on stainless steel, for the same deposition duration, appear smaller and irregular (Fig. 2b). This system has been studied in [41], revealing significant growth of carbon structures only at substrate temperatures above 575 °C. Modest growth observed in our case is in accordance with the applied conditions, which cannot provide such high substrate temperatures. The Raman modes attributed to carbon deposit observed on Ni-foam and on stainless steel are D (~1335 cm^{-1}), G (~1593 cm^{-1}) and 2D (~2649 cm^{-1}), and the low-intensity D‘ (1615 cm^{-1}), D+D‘ (2915 cm^{-1}) and 2D‘ (3205 cm^{-1}), typically observed in graphene-based structures (Fig. 2c). Well-pronounced G-band is an intrinsic feature of all sp^2 (graphitic) carbon, while D and D‘ are related to defects and disorders. Poor coverage of the stainless-steel surface with carbon nanostructures is also reflected in its Raman spectrum, i.e., there is a strong background due to light scattering from the stainless-steel substrate (raw Raman spectra can be found in the SI Fig. 1S). In addition to these substrates, the Cu substrate was also tested, however, no deposit was observed under the same operational conditions. This can be related to the lower adhesion energy of graphene on Cu ~ 0.72 Jm^{-2} as compared to the ~ 6.77 Jm^{-2} on Ni substrate [42]. Starting from these magnitudes average adhesion energy per surface atom can be estimated to be about 0.5 and 5 eV for Cu and Ni substrates, respectively. Considering the indicated energy values it can be concluded that the bonding between graphene and Ni substrate has covalent character in contrast to the van der Waals interactions with Cu.

3.1.2. Different pre-treatment of Ni-foam and Ni-foil

Furthermore, the influence of substrate pre-treatment on the VCN deposition process was also studied. Two cases were considered, i.e., substates with different surface morphologies Ni-foam and Ni foil. The deposition was performed on the previously annealed Ni-foam, and on the chemically etched Ni foil, both exposed to Ar plasma. In the case of Ni-foil annealed in air, thin and irregular deposition was observed, not suitable as electrode coating, therefore this case was not considered. The aim of the Ar plasma treatment was to perform cleaning of the substrate by ion sputtering, as well as to increase the substrate temperature, and to create roughness thus activating the surface. The Ar^+ ions are accelerated towards the dc biased substrate, resulting in surface sputtering that contributes to the removal of contaminants like water vapor, hydrocarbons etc., from the sample surface. However, in parallel to this process, mechanism of hydrocarbon growth in Ar plasma may also occur via the well-known effect of beam-enhanced polymerization [43–45]. Hydrocarbon molecules from residual gas are efficiently adsorbed on the substrate due to the high sticking coefficient. When exposed to Ar^+ bombardment, these molecules are dissociated, and the free radicals formed in this way cross-link and form, with time, inert polymer-like structures. Which of the two processes will dominate depends on the ion sputtering yield and the partial pressure of hydrocarbon species.

XPS analysis of the Ni-foam after the Ar plasma treatment, have demonstrated the following atomic ratios: O/C = 0.374, Ni/C = 0.714. The XPS of Ni 2p region obtained from the Ni-foam substrate treated with Ar plasma, includes the photoelectron doublet undoubtedly assigned to Ni^0, with its Ni $2p_{3/2}$ component centred at 852.6 eV and Ni $2p_{1/2}$ component + 17.1 eV apart (Fig. 2S). A fit of Ni 2p profile with Ni 2p spectra of reference samples of nickel in different oxidation states, led to the following relative weights: Ni^0 – 89.1 at%; $Ni(OH)_2$– 9.7 at%; and NiOOH – 1.2 at%. Oxygen is dominantly found as C-O, C=O, $Ni(OH)_2$, and NiOOH (see SI). The main peak in C 1 s region, centred at 284.6 eV is assigned to sp^2 C–C and C–H carbon, which implies that some graphitization of the deposited hydrocarbon layer could also be occurring (Fig. 2S). Therefore, under the conditions considered, the Ar plasma treatment led to additional hydrocarbon deposition, whilst the substrate oxide surface layer, grown due to the air exposure, was not removed.

The SEM and XPS analyses of the VCNs synthesized on Ni-foam at plasma conditions P=800 W, Q_{CH4} = 10 sccm, t = 60 min, U = -400 V, are shown in Fig. 2 d,e,f. It can be clearly seen from the SEM image (Fig. 2d) that vertically oriented structures are grown. The chemical composition analysis of VCNs on Ni foam by XPS analysis (Fig. 2 e,f) reveals the presence of carbon (67.8 at%), oxygen (28.0 at%), and Ni (4.2 at%). While the highly asymmetric shape of the C 1 s line is typical for graphitic carbon phases, its maximum position below 284 eV is a signature of poor electrical contact with the ground. Indeed, from the best fit of the Ni $2p_{3/2}$ line it can be concluded that the metallic bulk (the corresponding contribution is 17.7 % of the overall Ni signal) is covered by a thin layer of $Ni(OH)_2$ which is on the potential of + 1.4 V (Fig. 3S). When fitting the main contributions of the C 1 s line we applied the peak model suitable for sp^2-rich carbon, previously determined from the measurements of the highly oriented pyrolytic graphite. The dominant contribution is attributed to sp^2 carbon (64.4 %), followed by that of the sp^3 carbon or hydrocarbon contamination (17.1 %), C-O bonds (8.8 %), (C=O)-O- bonds (4.9 %) and finally a wide peak attributed to the π–π* system (4.9 %). Such bond identification, including the relative shifts due to the differential charging of different chemical phases, is justified by the fitting of the O 1 s line.

In another aspect, Ni foil was also used for the experiments to avoid surface oxidation of the substrate and to create roughness. VCNs were grown on Ni-foil at the plasma conditions P = 800 W, Q_{CH4} = 10 sccm, t = 60 min, U = -400 V (Fig. 3 g,h,i), and indeed, this sample showed the best XPS results in terms of oxygen contamination: it contained carbon (89.5 at%), oxygen (5.5 at%), and nickel (5 at%). The latter is also confirmed by the fitting of the C 1 s and Ni $2p_{3/2}$ line, showing much smaller relative contributions attributed to the bonds with oxygen. The C 1 s line was fitted to four contributions, with the most intense contribution attributed to sp^2 C–C bond (73.6 %), followed by sp^3 C–C (13.6 %), and C-OH (5.4 %). The fourth contribution (7.5 %) is the wide π–π* complex. The Ni 2p line has two contributions assigned to metallic Ni (80 % of the total Ni signal) and $Ni(OH)_2$ (Fig. 3S). This can also be seen in the oxygen 1 s line: 40 % $Ni(OH)_2$; the rest is C-OH. The presence of sp^2 C–C and the π–π* shake-up satellite are indications that graphene-like structures were synthesized.

This investigation reveals that substrate pre-treatment plays a very important role in the growth of VCNs. The air-exposed Ni-foam surface is passivated by the formation of NiO and $Ni(OH)_2$ surface layers, depending on the surface treatment (for instance, annealing in air). Graphene structures will not grow on such surfaces. The role of Ar plasma activation, and particularly chemical etching, is to make cracks and defects in such chemically inert layers. It is considered that nucleation and growth in the vertical direction will initiate only from these defective sites [10,22]. Therefore, the morphology of grown structures will strongly depend on the shape and size of these defects. To decrease the oxygen on the substrate, which interferes with the synthesized carbon nanostructures, chemical etching was performed. Although

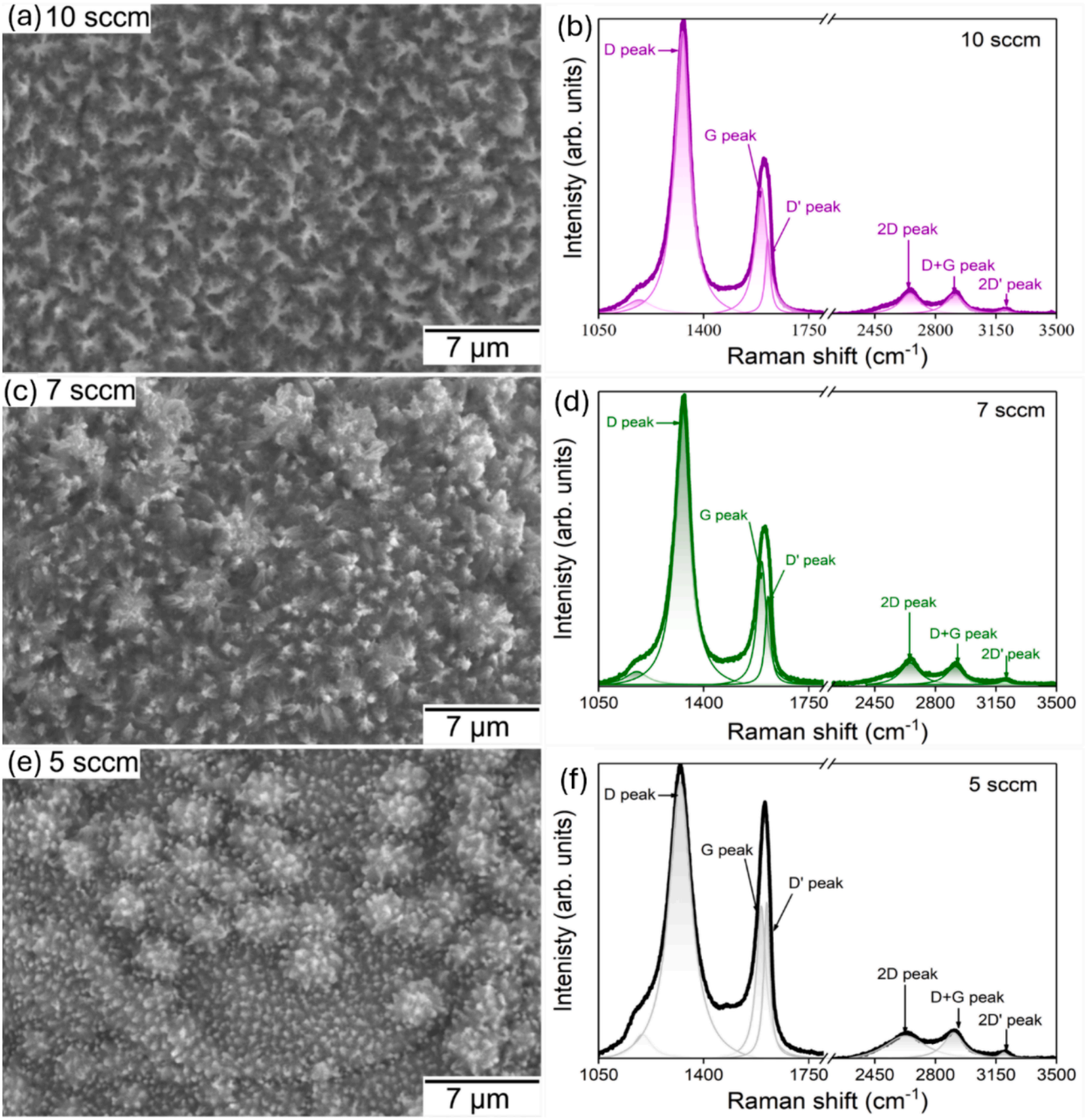

Fig. 3. Effect of methane flow rate on the morphology of vertical graphene nanostructures, SEM images and corresponding Raman spectra.

chemical etching removes this oxide layer, subsequent Ar plasma treatment creates both a similar hydrocarbon layer and defects. Therefore, Ar plasma treatment enables the processes of nucleation and growth of VCNs. Moreover, this hydrocarbon layer plays the role of a protective coating to prevent oxidation and corrosion of the underlying metal substrate [42]. Indeed, using chemically etched Ni-foil substrate, VCNs were grown with low relative oxygen content (5.5 at%) and with a high fraction of sp^2 carbon bonds (73.6 at%).

3.1.3. Influence of the negative bias voltage applied on the substrate

In general, the substrate surface is on negative potential with respect to plasma, which accelerates positive ions towards the surface. Effective control of particle fluxes and energies towards the targeted surfaces is crucial for governing the synthesis process. For this reason, additional dc biasing of the substrate located in plasma was introduced to shape the ions energy distribution via changing the substrate potential with respect to the local plasma potential. Therefore, the substrate bias voltage (its absolute value) was increased to enhance the ion bombardment effect, substrate temperature, nucleation and growth rate. It is to be noted the negative dc biasing provides vertical alignment of the carbon nanostructures. The influence of different substrate biasing on the surface morphology was monitored at different voltages (−200 and −400 V), while keeping the plasma parameters constant (Q_{CH4} = 10 sccm, P = 800 W, t = 60 min).

Well-aligned VCNs are grown at dc bias voltage of −200 V, whilst their lateral size increases at −400 V, as seen from SEM images (Fig. 2 j, k). The nanostructures grown at −200 V are densely packed and exhibit cone-like shapes, while the synthesis at −400 V leads to the lateral development into somewhat larger structures with turnstile-like morphology. This result demonstrates that control of the morphology

can be achieved by adjusting the dc negative bias voltage on the substrate. SEM images of cross-section of VCNs synthesized at different condition are shown in SI (Fig. 4S).

3.2. Influence of the plasma parameters

The effects of the plasma operational parameters, such as carbon precursoŕs flow rate, treatment time, and addition of H_2 gas, on the growth and morphology of the nanostructures were also studied.

3.2.1. Influence of the carbon precursor's flux

By investigating the substrate effects and bias voltage, optimal operational parameters for the VCN growth in methane plasma were found to be 800 W of microwave power, a bias voltage of –400 V, and a deposition time of 60 min. By keeping these parameters fixed, the methane flow rate (Q_{CH4}) was varied from 10 to 5 sccm. In all cases, the substrate surface was uniformly covered with the deposited nanostructures, however, with different morphologies (Fig. 3 a, c, e). Well-defined turnstile-like nanowalls (10 sccm) were transformed into thinner cone-like structures (7 sccm), while a further decrease of Q_{CH4} (5 sccm) yielded in small clustered nanostructures reminiscent of petal-like. In [46] VCN morphology change from nanofibers, nanowalls to interconnected nanowalls was observed with the decrease of the precursoŕs flow rate (paraxylene), which was associated with formation of defects at low flow rates. The structural quality of the synthesized nanostructures was analysed by Raman spectroscopy, an effective technique for investigating sp^2 and sp^3 hybridized carbon atoms. Each Raman spectrum in Fig. 3 (b,d,f) corresponds to an average spectrum of the spectra collected at different sample regions. The Raman spectra of the samples grown with 10 and 7 sccm (Fig. 3 b,d), exhibit peaks of graphene-like material: sharp G peak at approximately 1592 cm^{-1}, indicating the presence of crystalline graphene layers, the D peak at 1335 cm^{-1} that corresponds to defective graphene layers and finally low intensity 2D peak, which is demonstrative of graphene. The 2D' and D+D' bands can also be observed, implying presence of D' band at about 1614 cm^{-1}. The regions encompassing G and D bands were therefore fitted to three Lorentzian contributions (D, G and D' bands). The fittings reveal that the D' intensity is in some cases comparable to that of the G band. The fitting results of the G, D, D' and 2D bands are summarized in Table 1, showing similar results of the samples made with 10 and 7 sccm, while those taken from the 5 sccm sample differ mainly by the increased width of the D peak (Table 1). The D/D' ratio can be used to estimate the predominant type of defects in graphene structures [47]. The measured ratio in our samples is in the interval (1.78 – 2.82). Therefore, we can conclude that there are both on-site defects (due to nitrogen doping) and boundary defects (due to the finite size of the graphene planes). The higher position (1592 cm-1) of the G line compared to one in free standing graphene (1583 cm-1) suggests comprehensive stress and/or increased dopant density in VCN [48,49].

Similarly with the Raman spectra, the most significant difference in surface morphology is observed between the sample synthesized with 5 sccm and the other two samples: the former is characterized by much smaller structures. In many cases, in the pressure range considered (10^{-1}-10^{-2} mbar), the deposition rate increases with reducing the gas pressure [50]. The size of the grown structures depends on the density of the nucleation centres formed on the surface, which increases with the deposition rate.

At the same time, it is known that a smaller grain size is obtained with a higher deposition rate. Therefore, smaller size structures in the 5 sccm sample can be explained by reduced gas pressure (due to the lower CH_4 flow rate), and consequently by higher deposition rate.

At lower flow rates the deposited species will have longer relaxation time to form ordered structures, while increased CH_4 flows should lead to lower ordering (and consequently to the formation of disordered structures). Another explanation for the reduced ordering and smaller deposition rate can be related to the phenomena of CH_4 plasma interaction with carbon surfaces. Since the deposition and erosion of carbon-based materials are simultaneous and competing processes, the net deposition rate can be reduced by enhanced sputtering [51]. It is known that chemical sputtering is an important channel of carbon removal in

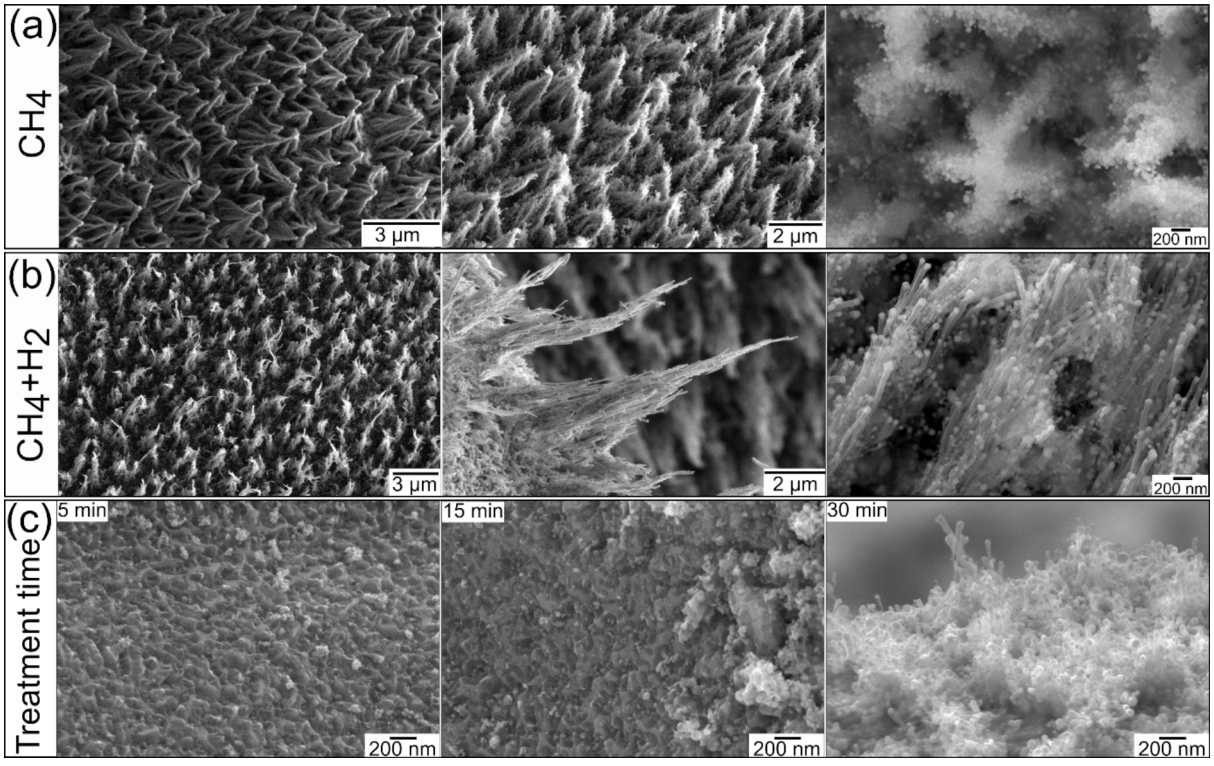

Fig. 4. Influence of H_2 gas as etching agent: a) SEM images of the sample grown with CH_4; b) SEM images of the sample grown with CH_4 and H_2 (CH_4:H_2 = 2:1) at different magnifications and observation angles; c) The morphology changes with plasma treatment duration (5, 15, and 30 min).

Table 1
Parameters from Raman spectra: intensity ratios and full width at half maximum (FWHM) of D, G, and 2D bands.

Sample	*Peak positions (cm^{-1})*				I_D/I_G	I_{2D}/I_G	$I_D/I_{D'}$	*FWHM*	*FWHM*	*FWHM*
	D	*G*	*D'*	*2D*				*D*	*G*	*2D*
10 sccm	1333	1592	1614	2645	1.991	0.173	2.82	51	39	197
7 sccm	1335	1593	1614	2649	1.938	0.180	2.70	49	37	166
5 sccm	1322	1591	1610	2629	1.883	0.157	1.78	90	38	251

hydrocarbon plasmas [52]. In CH_4 plasmas, in particular, the hydrogen atoms are the dominant reaction product, contributing significantly to the chemical sputtering of carbon. Thus, increased CH_4 flow in the plasma leads to increased flux of atomic hydrogen towards the substrate surface, where erosion of the carbon species occurs. At lower CH_4 flow the carbon growth channel dominates over the chemical sputtering, yielding in higher deposition rate i.e. thicker deposition layer. One can also expect that erosion processes are also generating defects, causing formation of smaller structures.

According to these results, the growth of vertically oriented nanostructures with $Q_{CH4} = 10$ sccm, P = 800 W, U = − 400 V, and t = 60 min is considered to be optimal, as evidenced by SEM and Raman analysis. This gas flow corresponds to the operation pressure of 0.3 mbar. In the further analyses, the samples were produced under these conditions. Besides, the ability to control the morphology of the synthesized VCNs by the precursor's flow rate was demonstrated.

3.2.2. *The effect of additional H_2 gas*

The role of buffer gas in the formation of carbon structures are also of interest in this research and therefore, the effect of hydrogen gas as an etching agent was also studied. It has been reported that the introduction of gases H_2, Ar, O_2, and H_2O improve the crystallinity and morphology of the vertical graphene structures [2]. This is ascribed to preferential etching of amorphous carbon by these gases with respect to the crystalline graphite phase [52,53]. The effect of H_2 during the plasma growth of VCNs is presented in Fig. 4 a,b. The SEM micrographs present distinguishable morphology differences of VCNs synthesized at the optimal operational conditions (P = 800 W, t = 60 min, U = -400 V) using CH_4 and CH_4 + H_2, respectively. The SEM images reveal that vertically oriented nanowalls were synthesized without the addition of H_2 (Fig. 4 a). The observed morphology is among the most common for graphene-like materials, i.e., turnstile-like with wall heights around 2–3 μm. High-resolution images show that the wall edges are terminated by fibre-like nano-structures. A top view of the SEM image (200 nm) of the sample clearly demonstrates the turnstile-like shape of the synthesized structures. While the insertion of H_2 with keeping the same CH_4 flow (CH_4:H_2 = 2:1) results in the growth of different nanostructures, i.e., nanofibres with a height of 5–8 μm (Fig. 4 b). Adding hydrogen to the gas discharge has a strong influence on the morphology of the synthesized structures: thick nanowalls were transformed into vertically oriented clusters of nanotubes. Such structures could be of potential interest as field electron emitters [54].

3.2.3. *Influence of the plasma treatment time*

The other important parameter is the plasma deposition time and the time-dependant morphology of the grown structures was studied by performing SEM analysis for different deposition times. The plasma operational parameters P = 800 W, Q_{CH4} = 10 sccm and U = -200 V, were kept constant and the deposition time varied from 5 to 30 min. After 5 min, the substrate was covered with a thin layer of a certain roughness and wave-like nanostructures (Fig. 4 c). At 15 min, carbon clusters are formed over the defective spots, and at 30 min small VCNs are grown. Therefore, under the conditions considered, about 30 min are necessary for the accomplishment of all critical steps, i.e., formation of structural defects on the substrate surface, creation of a thin hydrocarbon layer, nucleation, and growth of VCN.

All the obtained findings suggest that the plasma-enabled synthesis of carbon nanostructures is highly influenced by different factors such as substrate surface chemistry and plasma operational parameters. Better growth (higher deposition rate and higher ordering of the structures) of VCNs on the nickel substrate rather than on the stainless-steel indicates the effect of the catalytic activity of the substrate for the VCN growth. The catalytic characteristics of the nickel substrate enhance the diffusion of carbon in the substrate more than the stainless steel and stimulate the initial growth, which results in the final orientation and dimension of the VCN [55]. This investigation revealed that the presence of oxygen at the substrate surface reduces the quality of VCNs. From that perspective, a chemically stable metallic oxide layer (mainly consisting of Cr_2O_3 and various Fe oxides [56,57]) on stainless steel surface, could be responsible for the low coverage of the substrate with VCNs. Surface properties can be further enhanced by the activation (chemical etching and Ar plasma pre-treatment) to improve growth control. These processes create more surface defects on the substrate and allow the formation of more dangling bonds with the carbon dimer during the nucleation stage. A higher number of nucleation spots leads to the formation of uniformly grown densely packed VCN structures compared to the non-treated substrates. Besides the surface chemistry, the surface potential also influences the growth process. During the plasma treatment, energy and flux of bombarding ions towards the negatively biased substrate are increased, which leads to a higher concentration of surface defect sites i.e., to a higher number of nucleation sites. The final outcome is increased density of the nanostructures.

Besides the substrate properties, the plasma operational conditions are also key in the processes of growth of the vertical nanostructures. Among them, the flux rate of the precursor gas is one of the main factors defining the morphology of the final nanostructure. The deposition rate becomes lower with a higher precursor flow rate, ascribed to the higher etching rate due to high flow. The high flow rate also reduces the time available for reactive species to incorporate into the existing nucleation centres during the initial growth phases because of the higher density of species, leading to less ordered structures. Along with the precursor gas, the insertion of other gases also significantly influences the growth of carbon nanostructures. In this work, hydrogen was used as a supplementary gas for the continuous etching of amorphous carbon to improve the structural quality of the VCNs. During the initial growth process, the carbon dimers could be bonded via dangling bonds, some of which would be bonded through sp^3 bonding. The presence of hydrogen could eliminate the weakly bonded carbon atoms by the etching and, in turn, improve the crystalline features of the material. In this case, the addition of hydrogen is modifying the morphology from nanowalls to vertically aligned nanotubes.

Even though all the plasma operational parameters are directly involved in the growth of VCNs, systematic identification of each stage in VCN growth relies on time-dependent growth. The time-evolved growth of VCN could be demonstrated as follows: the carbon precursor was ionized and dissociated into ions and radicals in the initial stages. The nickel substrate featured point defects and dangling bonds through surface plasma interaction, where carbon deposition is initiated. During the nucleation, Ni slightly melted Ni nanoparticles formed with a thin carbon layer (5 min). The second stage began with the formation of carbon clusters over the defect spots. The growth continued, where the vertical dimension of the carbon nanostructures increased by the absorption of carbon atoms, forming a pillar-like structure. Along with the prolonged growth time, these clusters transform to branch-like

structures, forming densely packed VCNs on the substrate.

3.3. Post-synthesis N-doping

In order to tailor the electronic properties of the VCN, nitrogen doping of VCNs was performed using Ar/N_2 plasma in the same plasma reactor as used for the VCN deposition. The VCN structures grown on the Ni foil (Fig. 2 g,h,i) were doped with nitrogen at following plasma operational conditions: P = 600 W, z = 8 cm, Q_{Ar} = 45 sccm, Q_{N2} = 5 sccm, t = 3 min (Fig. 1 b) [27,28].

Surface characterization of the doped nanostructures (NVCN) by XPS revealed the presence of C, N, Ni, O, and Si at the surface. The SEM image and the relevant detailed regions of the XPS spectrum are shown in Fig. 5. The C 1 s photoelectron region was fitted with four peaks centred at: 284.4 eV attributed, mainly, to graphitic-like sp^2 C–C [36] and also to C–H; 286.1 eV attributed mainly to C-O, but most probably also including some sp^3 C–C and/or C–H (285 eV) and C-N (286 eV); 288.7 eV assigned to carboxylates and/or N-C=O; and 291.7 eV attributed to π–π^* energy losses features [58]. N 1 s was fitted with three peaks centred at 398.0 ± 0.1 eV, 399.5 ± 0.1, and 401.2 ± 0.1 eV attributed to pyridinic, pyrrolic, and quaternary nitrogen atoms, respectively [58]. The nitrogen relative amount is ~ 2.4 *at*%, and N/C=0.081. Additionally, the main doublet in Ni 2p (not shown) is no longer that assigned to Ni^0, as in the Ni-foam with no VCN. The Ni $2p_{3/2}$ main peak in NVCN is centred at 854.1 ± 0.1 eV, which is closer to Ni^{2+} species, namely $Ni(OH)_2$ [35].

3.4. Electrochemical studies

Deposition of a few micrometer thick VCN structures directly on the current collector allowed the use of material directly in the form of binder-free electrodes without any further electrode processing. Such assembly should provide sufficiently high electrical conductivity, which is critical for high-frequency applications.

The results of the electrochemical studies performed on VCN and NVCN structures are summarized in Fig. 6. Cyclic voltammetry (CV) studies performed on the two types of electrodes (Fig. 6 a) demonstrate quasi-rectangular shapes, with NVCNs having slightly higher current response. Such a result illustrates the potential of electrodes for EC applications.

Nyquist plots obtained from the EIS measurements of the two electrodes (Fig. 6 b-c) are similar, showing equivalent series resistances (ESR) of 87 and 92 mΩ for VCN and NVCN, respectively. Such low ESRs for both electrodes make them suitable in high frequency applications. Frequency dependence of the phase angle reveals quite high cut-off frequency (a frequency at which the phase angle reaches −45°) of about 4 kHz for both electrodes (Fig. 6 d) and the corresponding time constant τ_{RC} of 39 μs. This material has a lower cut-off frequency but also lower τ_{RC} than VCN reported in [59]. Besides, our structures have lower resistivity at the cut-off frequency (0.11 Ω vs. 0.67 Ω in [59]). It is interesting to mention that the work in [59] demonstrated the superiority of VCN structures in AC filtering with respect to horizontally and randomly grown structures. At the same time the respective phase angles values for VCN and NVCN electrodes at 100 Hz are −81.5° and −78.1°; the electrodes, deliver, respectively, capacitances of 481 and 477 μF (Fig. 6 e).

It is interesting to compare the ESR and the capacitance values obtained in this work with literature data obtained in similar conditions. Such comparison, for the frequency of 120 Hz concerning the results reported elsewhere [31–33,60–64] is presented in Fig. 6 f. The electrodes developed in this work display lower ESR and higher capacitance values compared to several other examples reported in the literature.

The excellent electrochemical performance, such as high capacitance, low ESR, and suitable phase angle, can be ascribed to the favourable structural and morphological properties of directly grown VCN and NVCN structures. The features that contribute to the enhancement of electrochemical properties include:

- the binder-free electrode preparation, which establishes the direct contact between the current collector and the active material to reduce the ohmic coupling at the current collector/material interface;
- high electrical conductivity of such structures that improves the charge transfer and efficient electrolyte interaction;

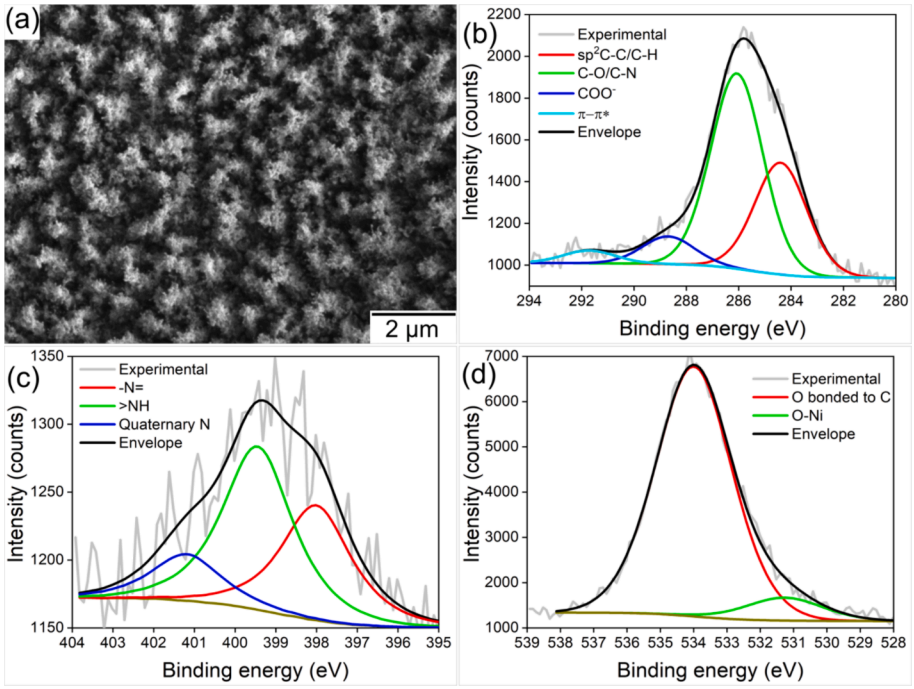

Fig. 5. Surface morphology and chemical composition analysis of NVCN – (a) top-view SEM micrograph, and high resolution XPS (b) C 1 s, (c) N 1 s and (d) O 1 s spectra.

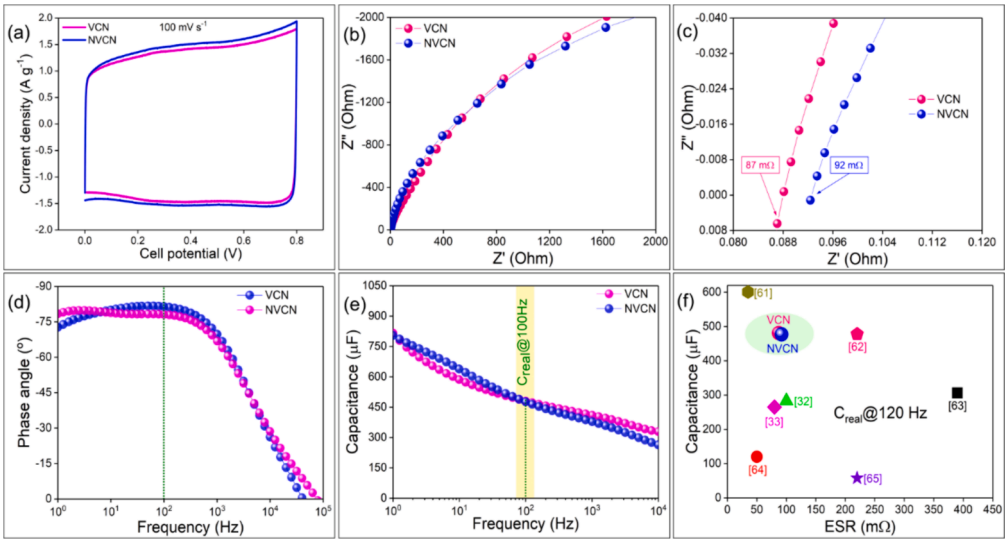

Fig. 6. Electrochemical performances of VCN and NVCN electrodes with 14 mm diameter (a) CV curves at a scan rate of 100 mV/s; (b-c) Nyquist plot; (d) Phase angle vs Frequency plot; (e) Capacitance vs Frequency plot and (f) Comparison between the capacitance vs ESR values in this work to some of the reported literature in carbon electrodes for high-frequency capacitors.

- the vertical morphology of the carbon nanostructures, which enlarges the effective area for enhanced electrode–electrolyte contact;
- design and doping in the plasma environment, which ensures the structural quality of the materials with a sufficient number of surface defects and stimulates the electrolyte interaction during the electrochemical processes.

Since a good capacitive response at high-frequency regions is the key to replacing the existing AECs in electric circuits for AC/DC conversion, the structure-controlled design of specific electrodes is crucial. Considering the excellent performances of plasma-designed electrodes at high frequencies, supercapacitor electrodes fabricated by such structures carry high potential to be used in electronic systems for alternating current line filtering applications as an alternative to AECs.

4. Summary

Growth of vertically oriented carbon nanostructures was achieved using a large-scale microwave plasma at low pressure conditions and methane as the carbon precursor. Optimal operational parameters for the vertical growth were established, as follows: $Q_{CH4} = 10$ sccm, P = 800 W, bias voltage of substrate U = − 400 V, deposition time 60 min. The effect of both the substrate and the plasma conditions on the nanostructure growth and morphology were investigated. The influence of the surface pre-treatment showed that chemical etching secures the lowest amount of oxygen impurities in the grown nanostructures, while the most versatile morphologies are obtained after annealing and Ar plasma pre-treatment of the substrate. Different deposition rates and morphologies were observed on Ni-foam and stainless steel substrates. Under the same conditions, due to the higher adhesion energy of carbon on Ni, thicker deposits were detected as compared with the ones on stainless steel. The addition of negative bias on the substrate, aiming to control the flux and energy of the bombarding ions, led to the synthesis of well-aligned nanowalls exhibiting turnstile-like morphology at a higher biasing voltage (−400 V). Additional tuning of the shape of the synthesized VCNs was achieved by the addition of H_2 in the plasma. Introducing H_2 changes the morphology from nanowalls towards nanotubes. Both structures are characterized by dominant sp^2 carbon bonds, as confirmed by XPS. With gas composition ratio CH_4:H_2 = 2:1, the growth of nanotubes with height 5–8 μm was achieved. Post-synthesis N-doping was obtained in the same plasma reactor system yielding 2.4 at% N and N/C = 0.081, as computed by XPS. Doped and pure VCNs synthesized under the optimal plasma conditions directly on the Ni-foil current collector and tested as high-frequency AC filtering capacitors showed good cut-off frequency of 4 kHz at which the phase angle is −45°. A suitable phase angle of −81.5° and −78.1° at 100 Hz, for doped and pure VCN, respectively were achieved and the overall capacitance was 481 and 477 μF at 100 Hz.

The excellent electrochemical performance, characterized by high capacitance, low equivalent series resistance, and appropriate phase angle, can be attributed to the favorable structural and morphological properties inherent in the directly grown vertically oriented carbon nanostructures providing binder-free electrode preparation. The used plasma approach to fabricate VCNs facilitates direct contact between the current collector and the active material by eliminating the need for binders, enhances the electrode's conductivity and charge transfer kinetics.

Furthermore, the design and doping of the nanostructures within the plasma environment ensure the structural quality of the materials, incorporating a sufficient number of surface defects. These defects play a crucial role in facilitating electrolyte interaction during electrochemical processes. By providing active sites for ion adsorption and desorption, surface defects enhance the electrode's electrochemical activity and capacitance. The used plasma method outclasses the conventional chemical approaches for electrode preparation by enabling precise control over nanostructure morphology and composition, leading to the formation of uniform and well-defined structures. Moreover, the plasma environment allows for rapid and efficient synthesis, reducing processing times and energy consumption. Additionally, plasma methods minimize the use of hazardous chemicals and by-products associated with traditional chemical synthesis routes.

In conclusion, plasma-enabled synthesis of vertically oriented carbon nanostructures offers a scalable and environmentally friendly approach for electrode design. The optimized processing parameters yield VCN-based electrodes with excellent high-frequency filtering performance, presenting a viable alternative to conventional electrolytic capacitors for high-frequency applications. Future work will focus on further optimizing the synthesis process and exploring additional functionalities of VCNs for diverse technological applications.

CRediT authorship contribution statement

N. Bundaleska: Writing – review & editing, Methodology, Investigation, Formal analysis, Data curation. **E. Felizardo:** Writing – review & editing, Validation, Software, Methodology, Investigation. **N.M. Santhosh:** Writing – review & editing, Writing – original draft, Formal analysis. **K.K. Upadhyay:** Writing – review & editing, Writing – original draft, Formal analysis. **N. Bundaleski:** Writing – review & editing, Methodology, Investigation, Formal analysis, Data curation. **O.M.N.D. Teodoro:** Writing – review & editing, Formal analysis, Data curation. **A. M. Botelho do Rego:** Writing – review & editing, Investigation, Funding acquisition, Formal analysis, Data curation. **A.M. Ferraria:** Writing – original draft, Methodology, Investigation, Formal analysis, Data curation. **J. Zavašnik:** Methodology, Investigation, Formal analysis, Data curation. **U. Cvelbar:** Writing – original draft, Methodology, Investigation, Formal analysis, Data curation. **M. Abrashev:** Writing – original draft, Methodology, Investigation, Formal analysis, Data curation. **J. Kissovski:** Writing – original draft, Methodology, Investigation, Formal analysis, Data curation. **A. Mão de Ferro:** Methodology, Investigation, Formal analysis, Data curation. **B. Gonçalves:** Resources, Project administration, Funding acquisition. **L.L. Alves:** Resources, Project administration, Funding acquisition. **M.F. Montemor:** Methodology, Investigation, Formal analysis, Data curation. **E. Tatarova:** Writing – review & editing, Writing – original draft, Supervision, Resources, Project administration, Methodology, Funding acquisition, Conceptualization.

Declaration of competing interest

The authors declare that they have no known competing financial interests or personal relationships that could have appeared to influence the work reported in this paper.

Data availability

Data will be made available on request.

Acknowledgments

This work was performed under the framework of the PEGASUS (Plasma Enabled and Graphene Allowed Synthesis of Unique nano-Structures) project, funded by the European Union's Horizon research and innovation program under grant agreement No 766894. MA and JK thank to the European Union-NextGenerationEU, through the.

National Recovery and Resilience Plan of the Republic of Bulgaria, project.

No BG-RRP-2.004-0008-C01 and INFRAMAT (National Roadmap for Research.

Infrastructure) supported by Bulgarian Ministry of Education and Science. Work partially funded by Portuguese FCT - Fundação para a Ciência e a Tecnologia, through projects UIDB/50010/2020 (https://doi.org/10.54499/UIDB/50010/2020), UIDP/50010/2020 (https://doi.org/10.54499/UIDP/50010/2020),LA/P/0061/2020 (https://doi.org/10.54499/LA/P/0061/2020); Eager project (PTDC/NAN-MAT/30565/2017) and iBB projects UIDB/04565/2020; UIDP/04565/2020; i4HB project LA/P/0140/2020 and Centro de Química Estrutural Research through projects UIDB/00100/2020 and UIDP/00100/2020 and Institute of Molecular Sciences, Associate Laboratory, through project LA/P/0056/2020. NB and OT thank the FCT for the funding support through projects UIDB/00068/2020 and UIDP/00068/2020. UC, NMS and JZ acknowledge the Slovenian Research Agency (ARIS) for the projects Z2-4467, J2-50074 and program No. P1-0417 and EU Graphene Flagship FLAG-ERA III JTC 2021 project VEGA (PR-11938) and M-ERA.NET 3 project ANGSTROM (The project is funded by Ministrstvo za visoko solstvo, znanost in inovacije – MVZI, Slovenia).

Appendix A. Supplementary data

Supplementary data to this article can be found online at https://doi.org/10.1016/j.apsusc.2024.161002.

References

[1] N. M. Santhosh, G. Filipic, E. Tatarova, O. Baranov, H. Kondo, M. Sekine, M. Hori, K. (Ken) Ostrikov, U. Cvelbar, Oriented Carbon Nanostructures by Plasma Processing: Recent Advances and Future Challenges, Micromachines 9 (2018) 565, doi:10.3390/mi9110565.

[2] Z. Zhang, C.-S. Lee, W. Zhang, Vertically Aligned Graphene Nanosheet Arrays: Synthesis, Properties and Applications in Electrochemical Energy Conversion and Storage, Adv. Energy Mater. 7 (2017) 1700678, https://doi.org/10.1002/aenm.201700678.

[3] O. Baranov, S. Xu, K. Ostrikov, B.B. Wang, U. Cvelbar, K. Bazaka, I. Levchenko, Towards universal plasma-enabled platform for the advanced nanofabrication: plasma physics level approach, Rev. Mod. Plasma Phys. 2 (2018) 4, https://doi.org/10.1007/s41614-018-0016-7.

[4] P. Sharma, V. Pavelyev, S. Kumar, P. Mishra, S.S. Islam, N. Tripathi, Analysis on the synthesis of vertically aligned carbon nanotubes: growth mechanism and techniques, Journal of Materials Science: Materials in Electronics 31 (2020) 4399–4443, https://doi.org/10.1007/s10854-020-03021-6.

[5] S. Alancherry, M.V. Jacob, K. Prasad, J. Joseph, O. Bazaka, R. Neupane, O. K. Varghese, O. Baranov, S. Xu, I. Levchenko, K. Bazaka, Tuning and fine morphology control of natural resource-derived vertical graphene, Carbon 159 (2020) 668–685, https://doi.org/10.1016/j.carbon.2019.10.060.

[6] W. Shi, D.L. Plata, Vertically aligned carbon nanotubes: production and applications for environmental sustainability, Green Chem. 20 (2018) 5245, https://doi.org/10.1039/C8GC02195C.

[7] S. Mori, M. Suzuki, Non-Catalytic Low-Temperature Synthesis of Carbon Nanofibers by Plasma-Enhanced Chemical Vapor Deposition in a $CO/Ar/O_2$ DC Discharge System, Applied Physics Express 2 (2009) 015003, https://doi.org/10.1143/APEX.2.015003.

[8] D.H. Seo, S. Kumar, K. Ostrikov, Control of morphology and electrical properties of self-organized graphenes in a plasma, Carbon 49 (2011) 4331, https://doi.org/10.1016/j.carbon.2011.06.0044339.

[9] D.H. Seo, Z.J. Han, S. Kumar, K. (Ken) Ostrikov, Structure-Controlled, Vertical Graphene-Based, Binder-Free Electrodes from Plasma-Reformed Butter Enhance Supercapacitor Performance, Adv. Energy Mater. 3 (2013) 1316–1323, https://doi.org/10.1002/aenm.201300431.

[10] K. (Ken) Ostrikov, I. Levchenko, U. Cvelbar, M. Sunkarad and M. Mozetic, From nucleation to nanowires: a single-step process in reactive plasmas, Nanoscale 2 (2010) 2012–2027, DOI: 10.1039/c0nr00366b.

[11] S.S. Swain, L. Unnikrishnan, S. Mohanty, S.K. Nayak, Carbon nanotubes as potential candidate for separation of H2-CO2 gas pairs, Int. J. Hydr. Energy 42 (2017) 29283–29299, https://doi.org/10.1016/j.ijhydene.2017.09.152.

[12] Z. Bo, Z. Wen, H. Kim, G. Lu, K. Yu, J. Chen, One-step fabrication and capacitive behavior of electrochemical double layer capacitor electrodes using vertically-oriented graphene directly grown on metal, Carbon 50 (2012) 4379–4387, https://doi.org/10.1016/j.carbon.2012.05.014.

[13] W.A. de Heer, A. Chatelain, D. Ugarte, A Carbon Nanotube Field-Emission Electron Source, SCIENCE 270 (1995) 1179–1180, https://doi.org/10.1126/science.270.5239.1179.

[14] L. Jiang, T. Yang, F. Liu, J. Dong, Z. Yao, C. Shen, S. Deng, N. Xu, Y. Liu, H.-J. Gao, Controlled Synthesis of Large-Scale, Uniform, Vertically Standing Graphene for High-Performance Field Emitters, Adv. Mater. 25 (2013) 250–255, https://doi.org/10.1002/adma.201203902.

[15] H. Borchert, F. Witt, A. Chanaewa, F. Werner, J. Dorn, T. Dufaux, M. Kruszynska, A. Jandke, M. Holtig, T. Alfere, J. Bottcher, C. Gimmler, C. Klinke, M. Burghard, A. Mews, H. Weller, J. Parisi, Vertically Oriented Carbon Nanostructures and Their Application Potential for Polymer-Based Solar Cells, J. Phys. Chem. C 116 (2012) 412–419, https://doi.org/10.1021/jp2095592.

[16] S. Chaitoglou, R. Amade, E. Bertran, Insights into the inherent properties of vertical graphene flakes towards hydrogen evolution reaction, Applied Surface Science 592 (2022) 153327, https://doi.org/10.1016/j.apsusc.2022.153327.

[17] S. Chaitoglou, R. Amade, R. Ospina, E. Bertran-Serra, Hybrid Nanostructured Compounds of Mo2C on Vertical Graphene Nanoflakes for a Highly Efficient Hydrogen Evolution Reaction, ACS Appl. Energy Mater. 6 (2023) 6120–6131, https://doi.org/10.1021/acsaem.3c00625.

[18] Z. Bo, Y. Yang, J. Chen, K. Yu, J. Yan, K. Cen, Plasma-enhanced chemical vapor deposition synthesis of vertically oriented graphene nanosheets, Nanoscale 5 (2013) 5180, https://doi.org/10.1039/C3NR33449J.

[19] S. Vizireanu, S. D. Stoica, C. Luculescu, L. C. Nistor, B. Mitu, G. Dinescu, Plasma techniques for nanostructured carbon materials synthesis. A case study: carbon nanowall growth by low pressure expanding RF plasma, Plasma Sources Sci. Technol. 19 (2010) 034016, DOI 10.1088/0963-0252/19/3/034016.

[20] H.J. Park, B.W. Ahna, T.Y. Kima, J.W. Lee, Y.H. Jung, Y.S. Choi, Y.I. Song, S.J. Suh, Direct synthesis of multi-layer graphene film on various substrates by microwave plasma at low temperature, Thin Solid Films 587 (2015) 8–13, https://doi.org/10.1016/j.tsf.2015.01.011.

[21] S. Hussain, E. Kovacevic, J. Berndt, N.M. Santhosh, C. Pattyn, A. Dias, T. Strunskus, M.-R. Ammar, A. Jagodar, M. Gaillard, C. Boulmer-Leborgne, U. Cvelbar, Low-

temperature low-power PECVD synthesis of vertically aligned graphene, Nanotechnology 31 (2020) 395604, https://doi.org/10.1088/1361-6528/ab9b4a.
[22] O Baranov, I Levchenko, S Xu, J W M Lim, U Cvelbar and K Bazaka, Formation of vertically oriented graphenes: what are the key drivers of growth? 2D Mater. 5 (2018) 044002, DOI:10.1088/2053-1583/aad2bc.
[23] L.X. Zhang, Z. Sun, J.L. Qi, J.M. Shi, T.D. Hao, J.C. Feng, Understanding the growth mechanism of vertically aligned graphene and control of its wettability, Carbon 103 (2016) 339–345, https://doi.org/10.1016/j.carbon.2016.03.029.
[24] E. Bertran-Serra, S. Rodriguez-Miguel, Z. Li, Y. Ma, G. Farid, S. Chaitoglou, R. Amade, R. Ospina, J.-L. Andújar, Advancements in Plasma-Enhanced Chemical Vapor Deposition for Producing Vertical Graphene Nanowalls, Nanomaterials 13 (2023) 2533, https://doi.org/10.3390/nano13182533.
[25] D. Tsyganov, N. Bundaleska, J. Henriques, E. Felizardo, A. Dias, M. Abrashev, J. Kissovski, A. M. Botelho do Rego, A. M. Ferraria, E. Tatarova, Simultaneous Synthesis and Nitrogen Doping of Free-Standing Graphene Applying Microwave Plasma, Materials 13 (2020) 4213, doi:10.3390/ma13184213.
[26] D. Tsyganov, N. Bundaleska, A. Dias, J. Henriques, E. Felizardo, M. Abrashev, J. Kissovski, A.M. Botelho do Rego, A.M. Ferraria, E. Tatarova, Microwave plasma-based direct synthesis of free-standing N-graphene, Phys. Chem. Chem. Phys. 22 (2020) 4772–4787, https://doi.org/10.1039/C9CP05509F.
[27] N. Bundaleska, N. Bundaleski, A. Dias, F.M. Dias, M. Abrashev, G. Filipič, U. Cvelbar, Z. Rakočević, Zh. Kissovski, J. Henriques, E. Tatarova, Microwave N_2-Ar plasmas applied for N-graphene post synthesis, Mater. Res. Express 5 (2018) 095605, https://doi.org/10.1088/2053-1591/aad7e9.
[28] K.K. Upadhyay, N. Bundaleska, M. Abrashev, N. Bundaleski, O.M.N.D. Teodoro, I. Fonseca, A. Mao de Ferro, R.P. Silva, E. Tatarova, M.F. Montemor, Free-standing N-Graphene as conductive matrix for Ni(OH)2 based supercapacitive electrodes, Electrochimica Acta 334 135592 (2020), https://doi.org/10.1016/j.electacta.2019.135592.
[29] N.M. Santhosh, G. Filipič, E. Kovacevic, A. Jagodar, J. Berndt, T. Strunskus, H. Kondo, M. Hori, E. Tatarova, U. Cvelbar, N-Graphene Nanowalls via Plasma Nitrogen Incorporation and Substitution: The Experimental Evidence, Nano-Micro Lett. 12 (2020) 53, https://doi.org/10.1007/s40820-020-0395-5.
[30] E. Van Hooijdonk, C. Bittencourt, R. Snyders, J.-F. Colomer, Functionalization of vertically aligned carbon nanotubes, Beilstein J. Nanotechnol. 4 (2013) 129–152, https://doi.org/10.3762/bjnano.4.14.
[31] N.M. Santhosh, K.K. Upadhyay, G. Filipic, J. Zavasnik, M.F. Montemor, U. Cvelbar, Widening the limit of capacitance at high frequency for AC line-filtering applications using aqueous carbon-based supercapacitors, Carbon 203 (2023) 686–694, https://doi.org/10.1016/j.carbon.2022.12.026.
[32] K. Sheng, Y. Sun, C. Li, W. Yuan, G. Shi, Ultrahigh-rate supercapacitors based on eletrochemically reduced graphene oxide for ac line-filtering, Scientific Reports 2 (2012) 247, https://doi.org/10.1038/srep00247.
[33] M. Cai, R.A. Outlaw, R.A. Quinlan, D. Premathilake, S.M. Butler, J.R. Miller, Fast Response, Vertically Oriented Graphene Nanosheet Electric Double Layer Capacitors Synthesized from C2H2, ACS Nano 8 (2014) 5873–5882, https://doi.org/10.1021/nn5009319.
[34] E. Tatarova, F.M. Dias, J. Henriques, C.M. Ferreira, Large-scale Ar and N2–Ar microwave plasma sources, J. Phys. D: Appl. Phys. 39 (2006) 2747–2753, https://doi.org/10.1088/0022-3727/39/13/018.
[35] M.C. Biesinger, B.P. Payne, L.W.M. Lau, A. Gerson, R. St, C. Smart, X-ray photoelectron spectroscopic chemical state quantification of mixed nickel metal, oxide and hydroxide systems, Surf. Interface Anal. 41 (2009) 324–332, https://doi.org/10.1002/sia.3026.
[36] A. Dias, N. Bundaleska, E. Felizardo, D. Tsyganov, A. Almeida, A. M. Ferraria, A. M. Botelho do Rego, M. Abrashev, Th. Strunskus, N. M. Santhosh, U. Cvelbar, J. Zavasnik, M.F. Montemor, M. M. Almeida, P. A. Carvalho, J. Kissovski, L. L. Alves, E. Tatarova, N-Graphene-Metal-Oxide(Sulfide) hybrid Nanostructures: Single-step plasma-enabled approach for energy storage applications, Chem. Eng. J. 430 (2022) 133153, DOI: 10.1016/j.cej.2021.133153.
[37] S. Ghosh, K. Ganesan, S.R. Polaki, T. Mathews, S. Dhara, M. Kamruddin, A. K. Tyagi, Influence of substrate on nucleation and growth of vertical graphene nanosheets, Appl. Surf. Sci. 349 (2015) 576–581, https://doi.org/10.1016/j.apsusc.2015.05.038.
[38] S.Y. Kim, Y.H. Joung, W.S. Choi, Growth properties of carbon nanowalls on glass substrates by a microwave plasma-enhanced chemical vapor deposition, Jpn. J. Appl. Phys. 53 (2014) 05FD09, DOI 10.7567/JJAP.53.05FD09.
[39] L. Zhang, Z. Shi, Y. Wang, R. Yang, D. Shi, G. Zhang, Catalyst-free growth of nanographene films on various substrates, Nano Res. 4 (2011) 315–321, https://doi.org/10.1007/s12274-010-0086-5.
[40] K. Ostrikov, E. Neyts, M. Meyyappan, Plasma nanoscience: from nano-solids in plasmas to nano-plasmas in solids, Adv. Phys. 62 (2013) 113–224, https://doi.org/10.1080/00018732.2013.808047.
[41] E. Bertran-Serra, A. Musheghyan-Avetisyan, S. Chaitoglou, R. Amade-Rovira, I. Alshaikh, F. Pantoja-Suarez, J.-L. Andújar-Bella, T. Jawhari, A. Perez-del-Pino, E. Gyorgy, Temperature-modulated synthesis of vertically oriented atomic bilayer graphene nanowalls grown on stainless steel by inductively coupled plasma chemical vapour deposition, Applied Surface Science 610 (2023) 155530, https://doi.org/10.1016/j.apsusc.2022.155530.
[42] W. Chang, S. Rajan, B. Peng, C. Ren, M. Sutton, C. Li, Adhesion energy of as-grown graphene on nickel substrates via StereoDIC-based blister experiments, Carbon 153 (2019) 699–706, https://doi.org/10.1016/j.carbon.2019.07.051.
[43] A. Dolgov, D. Lopaev, C.J. Lee, E. Zoethout, V. Medvedev, O. Yakushev, F. Bijkerk, Characterization of carbon contamination under ion and hot atom bombardment in a tin-plasma extreme ultraviolet light source, Appl. Surf. Sci. 353 (2015) 708–713, https://doi.org/10.1016/j.apsusc.2015.06.079.
[44] E.H. Hirsch, The growth of carbonaceous contamination on surfaces undergoing ion bombardment, J. Phys. D: Appl. Phys. 10 (1977) 2069, https://doi.org/10.1088/0022-3727/10/15/010.
[45] I. Figueiredo, N. Bundaleski, O.M.N.D. Teodoro, K. Jousten, C. Illgen, Influence of ion induced secondary electron emission on the stability of ionisation vacuum gauges, Vacuum 184 (2021) 109907, https://doi.org/10.1016/j.vacuum.2020.109907.
[46] K. Lehmann, O. Yurchenko, G. Urban, Effect of the aromatic precursor flow rate on the morphology and properties of carbon nanostructures in plasma enhanced chemical vapor deposition, RSC Adv. 6 (2016) 32779–32788, https://doi.org/10.1039/C6RA02999J.
[47] S. Meskinis, A. Vasiliauskas, A. Guobiene, M. Talaikis, G. Niaura, R. Gudaitis, The direct growth of planar and vertical graphene on Si(100) via microwave plasma chemical vapor deposition: synthesis conditions effects, RSC Adv. 12 (2022) 18759–18772, https://doi.org/10.1039/d2ra02370a.
[48] J.E. Lee, G. Ahn, J. Shim, Y. Sik Lee, S. Ryu, Optical separation of mechanical strain from charge doping in graphene, 1024, Nat. Commun. 3 (2012), https://doi.org/10.1038/ncomms2022.
[49] R. Gudaitis, A. Lazauskas, Š. Jankauskas, Š. Meškinis, Catalyst-Less and Transfer-Less Synthesis of Graphene on Si(100) Using Direct Microwave Plasma Enhanced Chemical Vapor Deposition and Protective Enclosures, Materials 13 (2020) 5630, https://doi.org/10.3390/ma13245630.
[50] A. Zendehnam, M. Ghanati, M. Mirzaei, Study and comparison of deposition rates, grain size of Ag and Cu thin films with respect to sputtering parameters, and annealing temperature, J. Physics: Conf. Series 61 (2007) 1322–1325, https://doi.org/10.1088/1742-6596/61/1/261.
[51] T. Schwarz-Selinger, C. Hopf, C. Sun, W. Jacob, Growth and erosion of amorphous carbon (a-C:H) films by low-temperature laboratory plasmas containing H and N mixtures, J. Nuc. Mat. 363–365 (2007) 174–178, https://doi.org/10.1016/j.jnucmat.2007.01.005.
[52] W. Jacob, C. Hopf, M. Schlüter, Chemical sputtering of carbon materials due to combined bombardment by ions and atomic hydrogen, Phys. Scripta T 124 (2006) 32–36, https://doi.org/10.1088/0031-8949/2006/T124/007.
[53] C.F. Adame, E. Alves, N.P. Barradas, P.C. Pinto, Y. Delaup, I.M.M. Ferreira, H. Neupert, M. Himmerlich, S. Pfeiffer, M. Rimoldi, et al., Amorphous carbon thin films: Mechanisms of hydrogen incorporation during magnetron sputtering and consequences for the secondary electron emission, J. Vac. Sci. Technol. A 41 (2023) 043412, https://doi.org/10.1116/6.0002759.
[54] B.B. Wang, K. Ostrikov, T. van der Laan, K. Zheng, J.J. Wang, Y.P. Yan, X.J. Quan, Carbon nanorods and graphene-like nanosheets by hot filament CVD: growth mechanisms and electron field emission, J. Mater. Chem. C 1 (2013) 7703, https://doi.org/10.1039/C3TC30750F.
[55] J. Wintterlin, M.-L. Bocquet, Graphene on metal surfaces, Surface Science 603 (2009) 1841–1852, https://doi.org/10.1016/j.susc.2008.08.037.
[56] E. Gardin, S. Zanna, A. Seyeux, A. Allion-Maurer, P. Marcus, XPS and ToF-SIMS characterization of the surface oxides on lean duplex stainless steel – Global and local approaches, Corrosion Science 155 (2019) 121–133, https://doi.org/10.1016/j.corsci.2019.04.039.
[57] S. J. Kerber, J. Tverberg, AES and XPS analysis of the passivation layer on stainless steel can help determine how well it will resist corrosion, ADVANCED MATER.& PROC., Corpus ID: 171039 (2000) 33-36, http://www.materialinterface.com/wp-content/uploads/2014/11/Stainless-steel-review-Matl-Interface.pdf.
[58] G. Beamson, D. Briggs, High Resolution XPS of Organic Polymers, the Scienta ESCA300 Database, Wiley, Chichester, 1992.
[59] L. Wang, Z. Li, M. Song, C. Xu, Z. Liu, S. Jia, X. Li, J. Liu, L. Meng, Z. Wang, X. Wang, Enabling directional ion transport over graphene electrode surfaces for kilohertz electrochemical capacitors, Electrochimica Acta 368 (2021) 137561, https://doi.org/10.1016/j.electacta.2020.137561.
[60] Y. Rangom, X. (Shirley) Tang, L.F. Nazar, Carbon Nanotube-Based Supercapacitors with Excellent ac Line Filtering and Rate Capability via Improved Interfacial Impedance, ASC, Nano 9 (2015) 7248–7255, https://doi.org/10.1021/acsnano.5b02075.
[61] Q. Zhou, M. Zhang, J. Chen, J.-D. Hong, G. Shi, Nitrogen-Doped Holey Graphene Film-Based Ultrafast Electrochemical Capacitors, ACS Appl. Mater. Interfaces 8 (2016) 20741–20747, https://doi.org/10.1021/acsami.6b05601.
[62] Z. Zhang, M. Liu, X. Tian, P. Xu, C. Fu, S. Wang, Y. Liu, Scalable fabrication of ultrathin free-standing graphene nanomesh films for flexible ultrafast electrochemical capacitors with AC line-filtering performance, Nano Energy 50 (2018) 182–191, https://doi.org/10.1016/j.nanoen.2018.05.030.
[63] M. Cai, R.A. Outlaw, S.M. Butler, J.R. Miller, A high density of vertically-oriented graphenes for use in electric double layer capacitors, CARBON 50 (2012) 5481–5488, https://doi.org/10.1016/j.carbon.2012.07.035.
[64] Y. Yoo, S. Kim, B. Kim, W. Kim, 2.5 V compact supercapacitors based on ultrathin carbon nanotube films for AC line filtering, J. Mater. Chem. A 3 (2015) 11801, doi: 10.1039/C5TA02073E.